

Additional file

Simulation of great earthquakes along the Nankai Trough: Reproduction of event history, slip areas of the Showa Tonankai and Nankai Earthquakes, heterogeneous slip-deficit rates, and long-term slow slip events

HIROSE F¹, MAEDA K¹, FUJITA K², KOBAYASHI A¹

¹Meteorological Research Institute, Japan Meteorological Agency, 1-1 Nagamine, Tsukuba, Ibaraki 305-0052, Japan

²Seismology and Volcanology Department, Japan Meteorological Agency, 3-6-9 Toranomom, Minato-ku, Tokyo, 105-8431, Japan

Section S1 shows the occurrence history of all earthquakes during 4400 years in our best model. Section S2 describes in detail the parameter tuning to obtain the best model: Section S2.1 for reproduction of rupture starting points; Section S2.2 for time lag between Tokai/Tonankai and Nankai earthquakes; Section S2.3 for along-strike extent of rupture areas, the Showa Tonankai and Nankai earthquakes, and the Hyuganada earthquake; and Section S2.4 for parameter tuning to reproduce the slip-deficit rate distribution.

S1. Occurrence history of simulated earthquakes

Figure S1 shows the time evolution of simulated slip velocity and cumulative slip displacement on the Nankai Trough plate boundary at reference points 1–7 and 12 (Fig. 4e, f). We judged an event to be coseismic when slip velocity in any cell reached 0.1 m/s, even if it did not reach 0.1 m/s at the reference points. Coseismic events occurred at intervals of 400–600 years at Suruga Bay (point 1). Coseismic events at point 2 occurred more frequently, at alternating intervals of 100–150 and 200–400 years. Earthquakes on the Tonankai segment (point 3) and the Nankai segment (point 4) occurred at intervals of 100–200 years as paired events; usually the Nankai earthquake followed the Tonankai earthquake after a short time lag, but sometimes they occurred simultaneously. The Tonankai earthquake at S2169 was an unpaired event (point 3). In the shallower part of the seismogenic zone off Shikoku (point 5), coseismic slip occurred at intervals of 100–300 years. Coseismic slip in northern Hyuganada (point 6) occurred with almost the same frequency and timing as earthquakes at point 4. At point 6, aseismic slip was simulated in the latter half of interseismic periods. Southern Hyuganada (point 7) generally had stable sliding, an effect of the large L , even where $a - b < 0$. In the deeper part of the seismogenic zone (point 12), where $a - b > 0$, stable sliding and afterslip was associated with events that ruptured the seismogenic zone.

Figure S2 shows the coseismic slip distribution on the plate interface for each of the 106 events in our simulation, and **Figure S3** summarizes their occurrence times and source regions. In the area east of the Kii Peninsula, events with M_w 7.9–8.4 ruptured segments C–D, C–E, and C–F, which correspond to Showa-, Hiei-, and Ansei-type events, respectively. In this area, the starting points of Tokai/Tonankai earthquakes (stars) were only in segment C; they were frequently at its southwestern edge, as in the case of the 1944 Showa Tonankai earthquake, and sometimes on the deeper part of the plate boundary. In the area west of the Kii Peninsula, events with M_w 8.1–8.6 ruptured the deeper part of segments A–B (Showa-type), entire segments A–B (Ansei- or quasi-Showa-type), and segments Z–B (Hiei-type). Earthquake starting points in this area were only in segment B; they were frequently at its southeastern edge, as in the case of the 1946 Showa Nankai earthquake, and sometimes on the deeper part of the plate boundary.

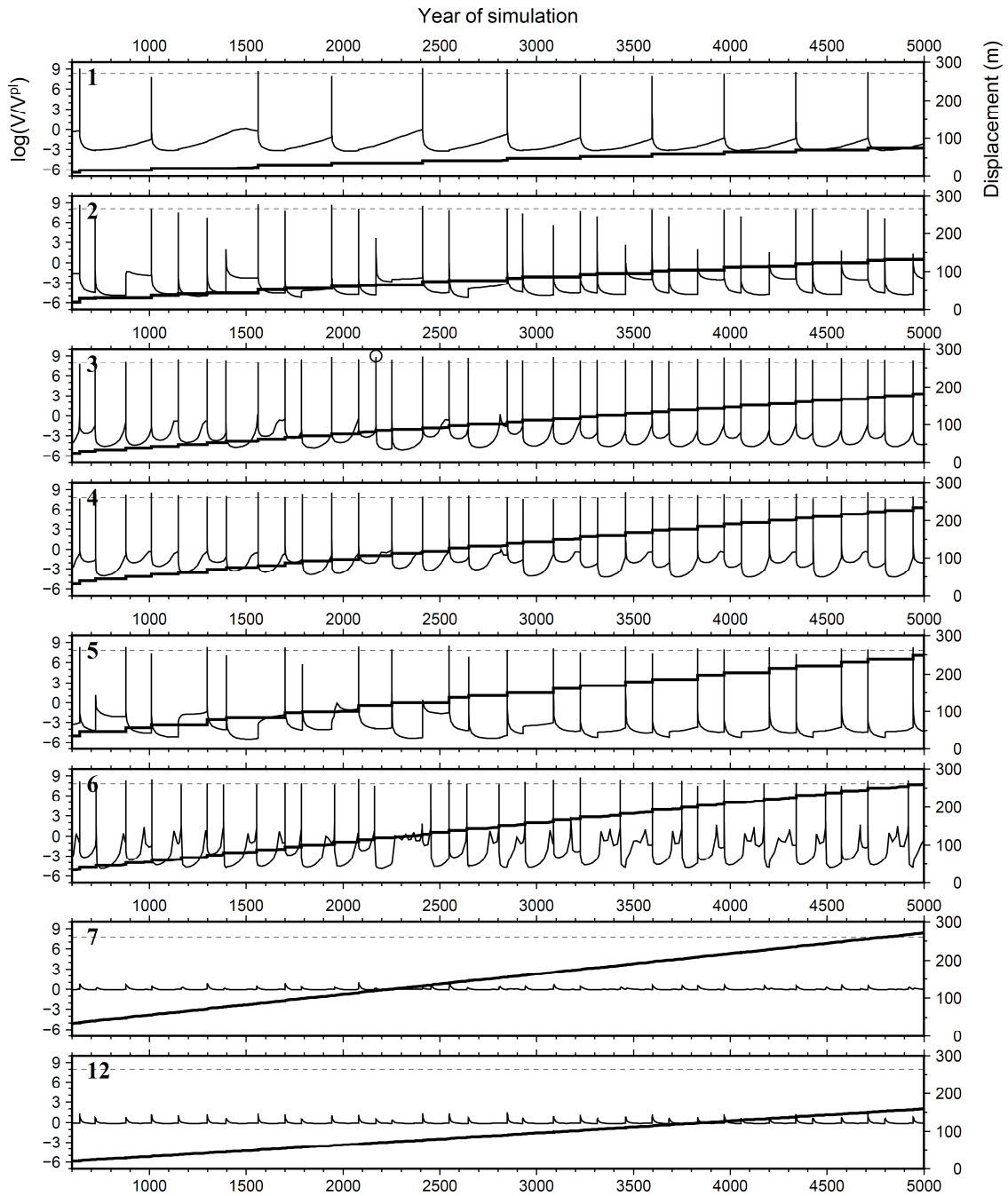


Fig. S1 Time evolution of slip velocity normalized by the plate convergence rate (thin line) and cumulative slip displacement (thick line) at points 1–7 and 12 in Figure 4e, f. Horizontal dashed lines correspond to a slip velocity of 0.1 m/s, the threshold of an earthquake. The circle in panel 3 denotes the unpaired Tonankai earthquake of event 39.

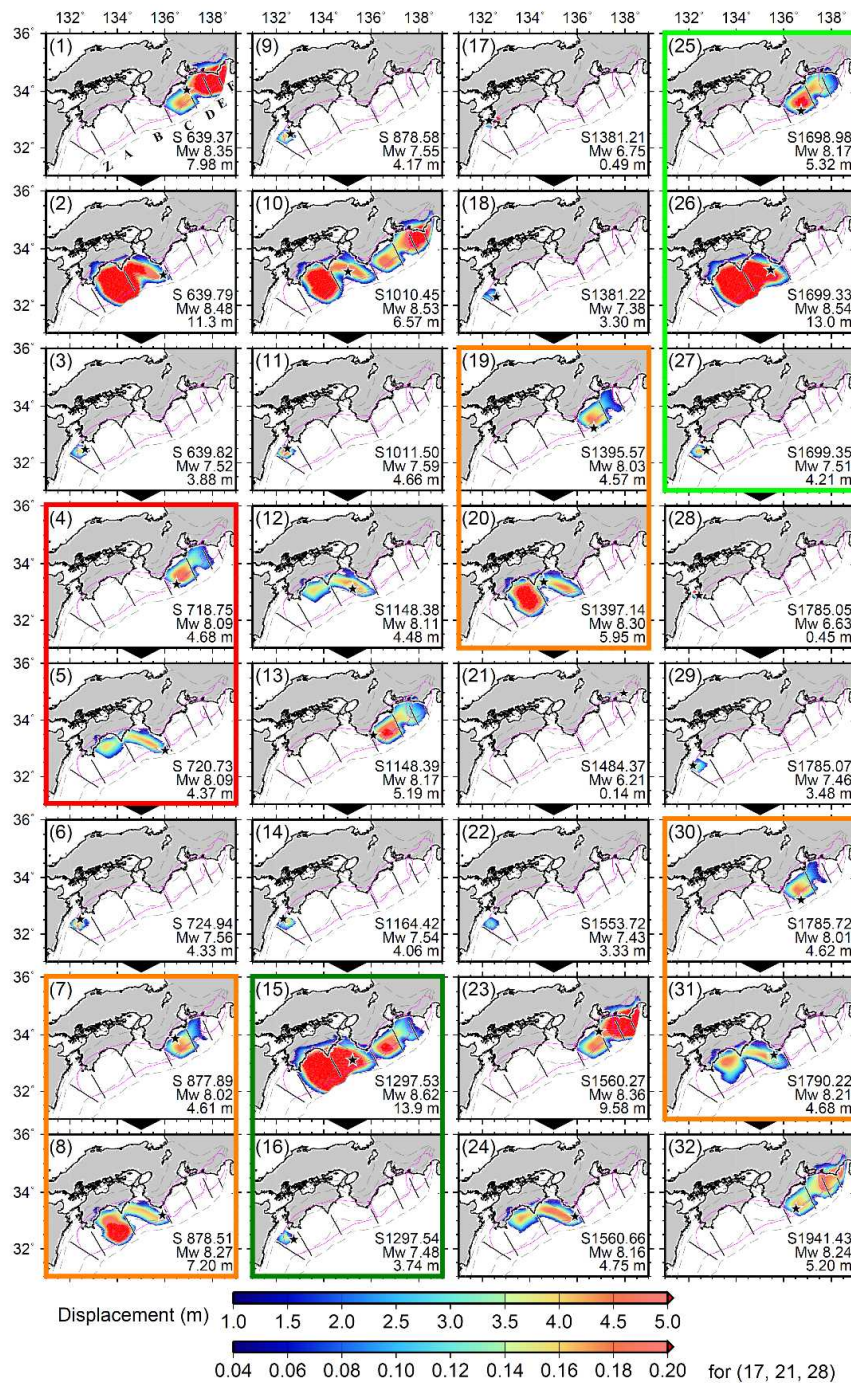


Fig. S2 Slip distribution for all events in our simulation. Stars indicate rupture initiation points. In each plot, the event number is at upper left, and the numbers at lower right are the elapsed years in the simulation (S600–S5000), the moment magnitude, and the maximum slip displacement. Colors of the borders correspond to the following event class: red, Showa; blue, Ansei; dark green, Hoei; orange, quasi-Showa; light green, quasi-Hoei; purple, isolated Tonankai types. Note that displacements for some events use a different color scale.

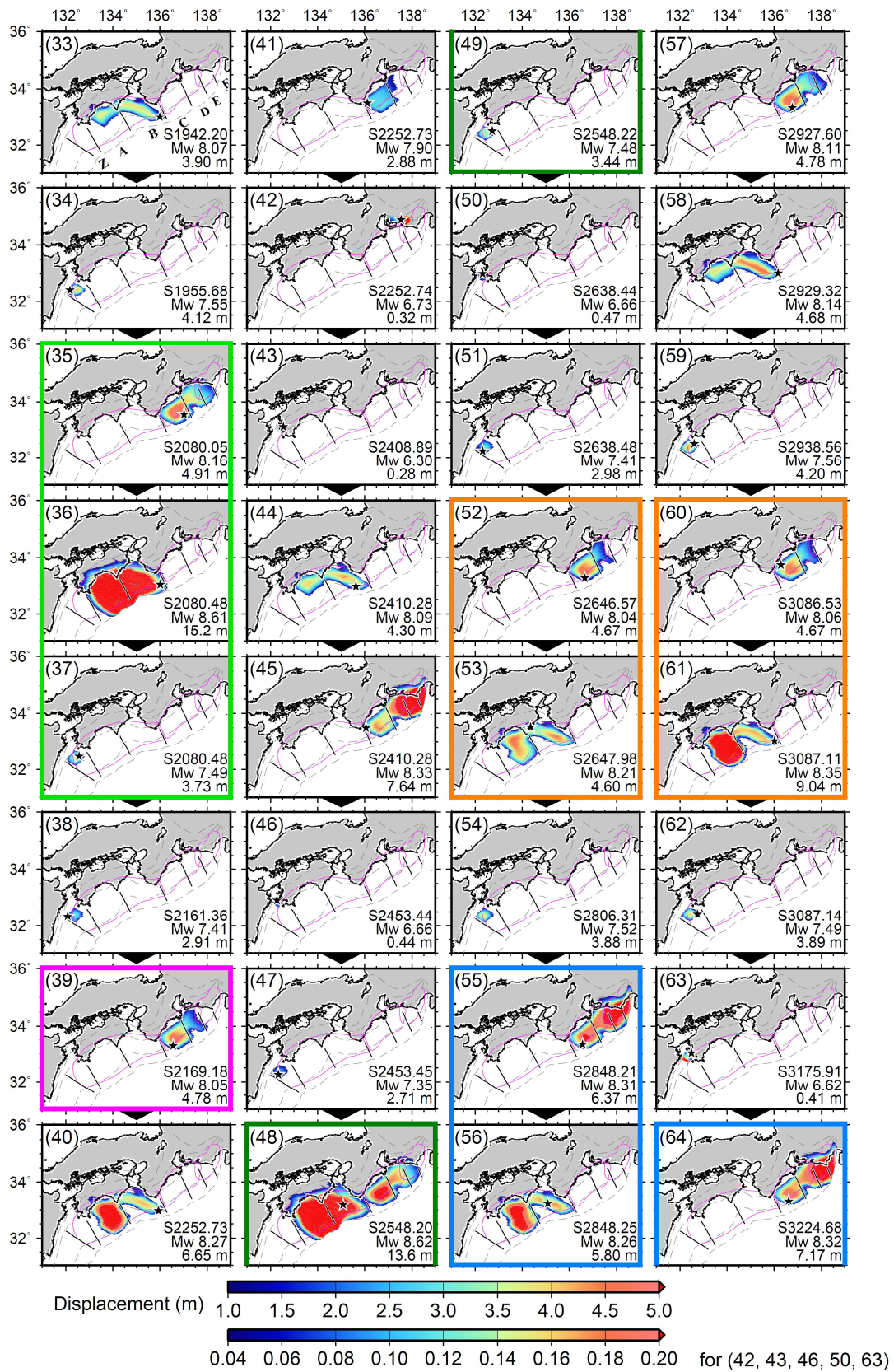


Fig. S2 Continued.

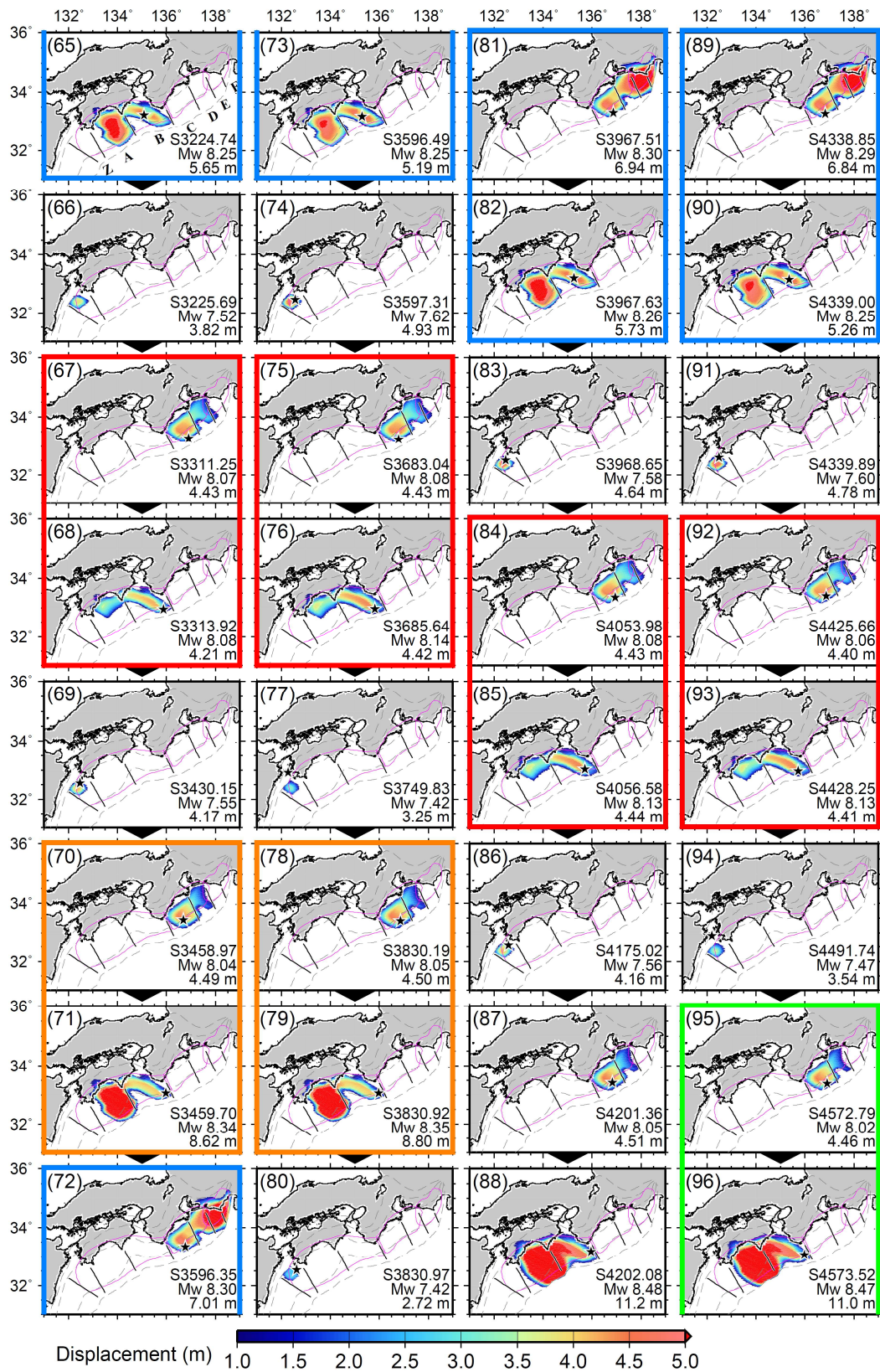


Fig. S2 Continued.

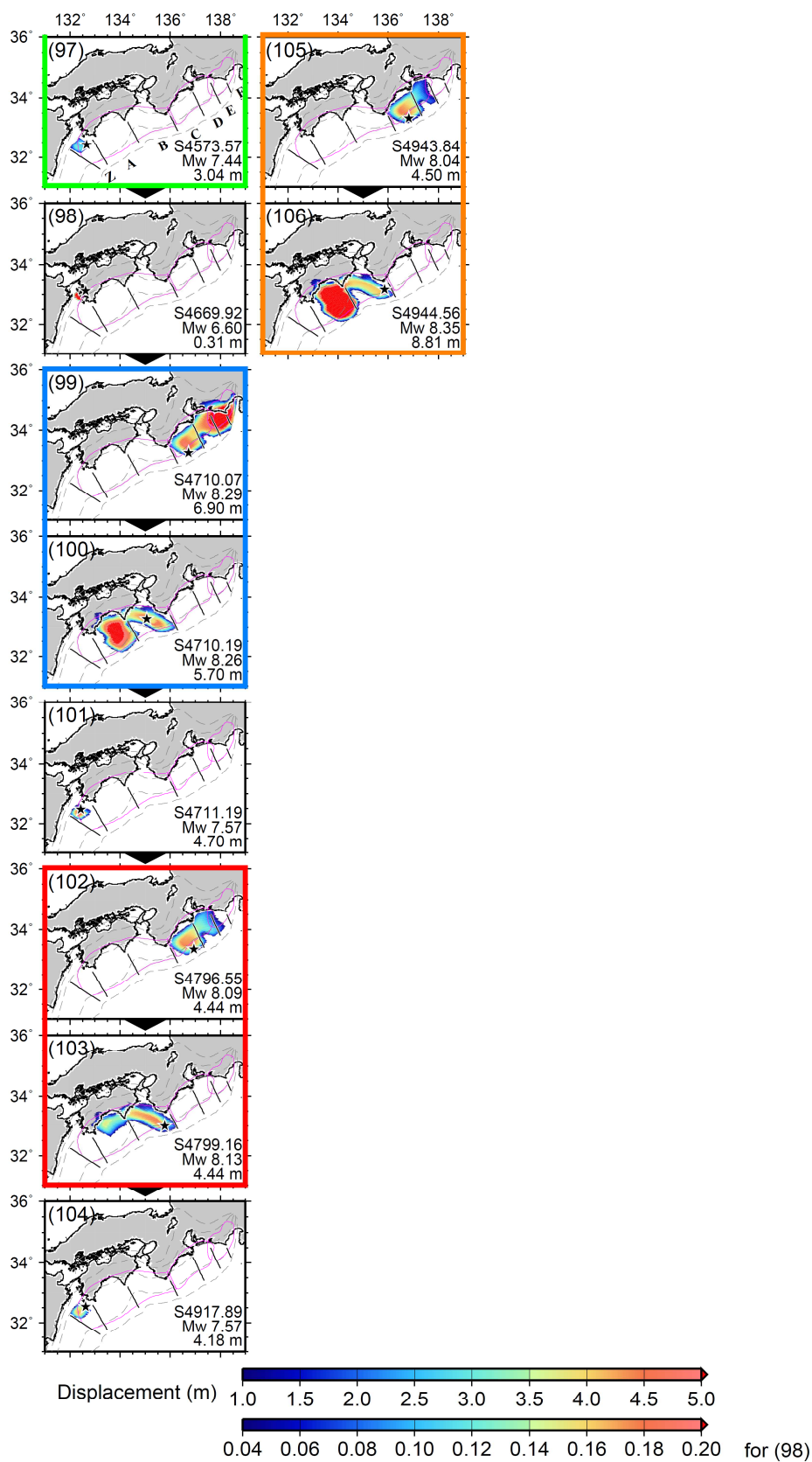


Fig. S2 Continued.

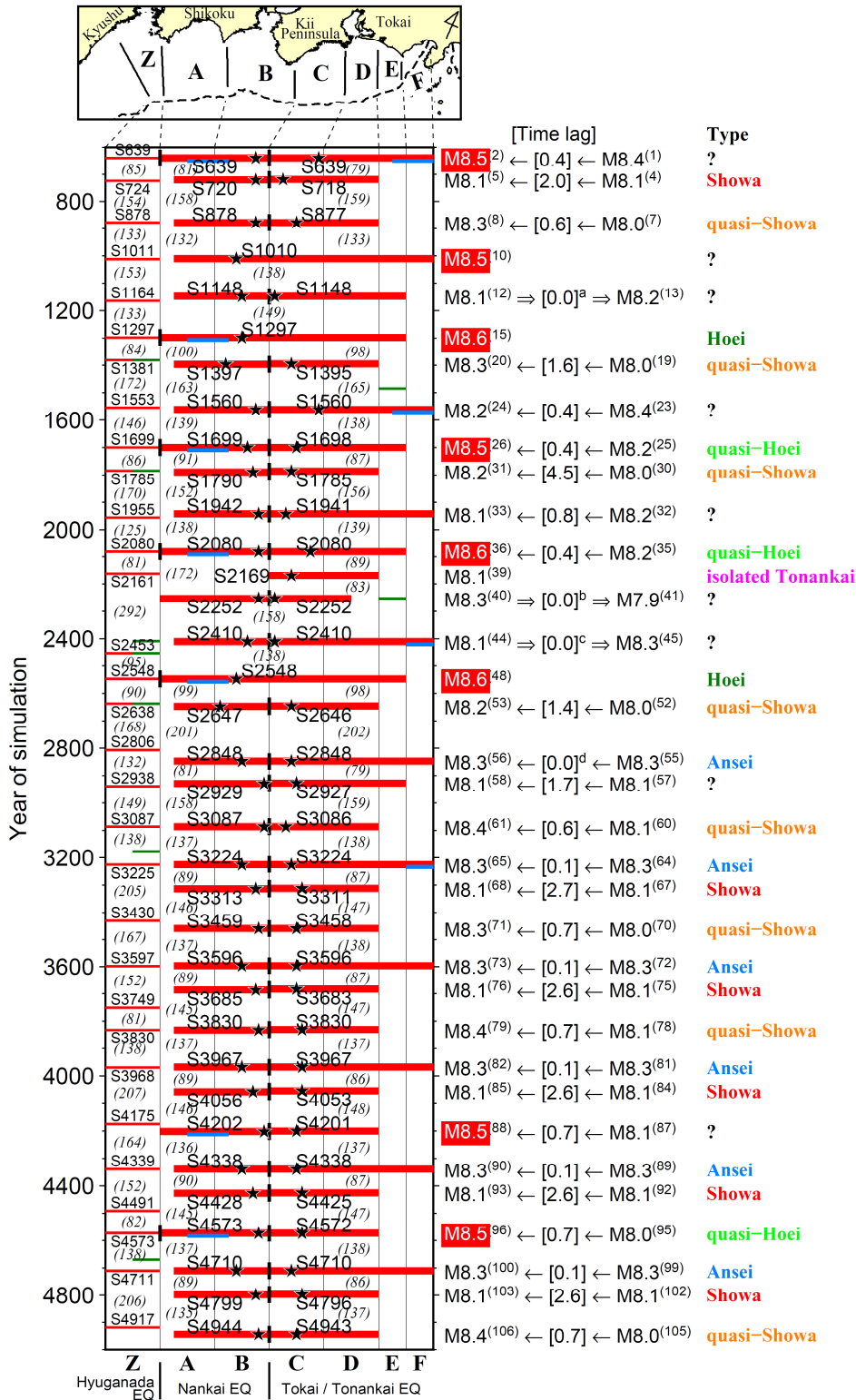


Fig. S3 Occurrence times and source regions of great Nankai Trough earthquakes during the years of our simulation (S600–S5000). See Figure 6 for details of this diagram. Superscripts a–d mean time lags of 1 day, 2 days, 1 day, and 2 weeks, respectively.

S2. Parameter tuning

We obtained the best model (**Fig. 4, Table 2**) as a result of changing the parameter values and adjusting the position and size of the asperity by trial and error. **Table S1** lists the ranges of parameters we tested at representative points 1–12. This section supplements the parameter tuning process.

S2.1. Reproduction of rupture starting points

First, we tuned characteristic displacement L with σ^{eff} set to 30 MPa (see Section 5.4). We took into consideration the hierarchical asperity model (Hori et al. 2009; Hyodo and Hori 2013) in which an area with small L is surrounded by an area with large L . This model shows that areas with various rupture conditions, such as a large- L area, can become a barrier and an asperity. In a simulation model for occurrence patterns of great earthquakes along the Japan Trench incorporating surrounding area with large L (Fujita et al. 2018), the reproducibility of afterslip of the M_w 9.0 2011 Tohoku earthquake was high when the background area outside the seismic asperity had a value of $L = 7.5$ m.

We started by conducting simulations (cases 1-1 to 1-6) that assigned uniform values of L (0.05, 0.06, 0.08, 0.10, 0.12, or 0.14 m) at depths of 5–20 km on the plate boundary in an area extending from the Tokai district to northern Hyuganada (**Fig. S4a, Table S2**). In all cases, only mega-earthquakes that ruptured the whole area occurred cyclically. **Figure S4a** shows starting points of earthquakes for the tenth event in the six simulations, which were located off Cape Ashizuri under relatively low L (0.05 and 0.06 m) and off Cape Shiono under large L (0.08–0.14 m). Because the plate convergence rate increases to the southwest (**Fig. 4c**), it can be said interplate coupling tends to weaken toward the southwest. On the other hand, in the area off Cape Shiono, where the slab dip angle is steep and the seismogenic zone is narrow, stress concentration also tends to increase due to stable sliding in the up-dip and down-dip of the seismogenic zone (e.g., Takayama et al. 2008). The size of L controls the size of the nucleation area h^* ; thus, when h^* is small, rupture is more likely to occur off Cape Ashizuri where plate convergence is faster (**Fig. S5**), and when h^* is large, rupture takes more time to occur and is more likely to start off Cape Shiono where the stress concentration is accelerated after the contact of up-dip and down-dip stable sliding (**Fig. S6**). The recurrence interval T_r increased with L (**Table S2**) because nucleation size h^* is proportional to L . Because the 1944 Tonankai and 1946 Nankai earthquakes occurred off Cape Shiono, if the time

lag (0–3 years) between Tokai/Tonankai and Nankai earthquakes (target phenomenon 1c) is ignored and we adopt a first approximation model in which ruptures spread bilaterally from off Cape Shiono (e.g., Hirose and Maeda 2013), we should adopt L with 0.08 m or more.

S2.2. Time lag between Tokai/Tonankai and Nankai earthquakes

In the historical record, Tokai/Tonankai earthquakes precede Nankai earthquakes with a time lag (target phenomenon 1c). Taking into consideration that the occurrence interval increases with L when $(b - a)\sigma^{\text{eff}}$ is uniform (Stuart 1988), as shown in Section 5.5, we ran a set of five simulations (cases 2-1 to 2-5) that assigned a smaller L to the area east of Cape Shiono than to the area west of the cape to reproduce this time lag. We fixed L in the eastern area at 0.05 m and changed L in the western area to 0.1, 0.2, 0.4, 0.6, and 0.8 m (**Fig. S4b, Table S3**). In all cases, earthquake starting points were at the eastern edge of the study area and off Cape Shiono without a time lag. At $L = 0.4$ m, a Nankai earthquake occurred once for every three Tonankai earthquakes, and no Nankai earthquake appeared at larger L values, perhaps because the nucleation size was greater than the asperity size. Because of the length-to-width ratios that we set for asperities, the nucleation size tended to be large (Kato 2003). **Figure S4b** and **Table S3** show starting points of earthquakes for the tenth and eleventh events in our simulations.

We could not reproduce the time lag when only L differed between the eastern and western sides. Therefore, we left L equal on both sides and added a belt-shaped area off Cape Shiono with a large L (**Fig. S4c, d, Table S4**) in hopes that it would generate a time lag by acting as a barrier to rupture (e.g., Hirose and Maeda 2013). We then assigned three values of L (0.08, 0.10, or 0.12 m) to the seismogenic zone of the whole area and three values of L (1.0, 3.0, or 7.5 m) to the belt-shaped area off Cape Shiono, which was either 15 km or 25 km wide, for a total of 18 cases (**Table S4**). The results confirmed that a time lag occurred between Tokai/Tonankai and Nankai earthquakes when there was a belt-shaped area of large L (see **Fig. 4c, d** for the starting points of the tenth paired events). When paired events occurred at two different time lags, the starting points of the paired events are shown in **Fig. S4c, d**, and the range of time lags is shown in **Table S4**. The time lag increased when the belt-shaped area was wider and when the contrast in L between the belt and the seismogenic zone was greater.

In these simulations, the Tokai/Tonankai earthquake tended to precede the Nankai earthquake when $L = 1.0$ m in the belt, but the opposite occurred when $L = 3.0$ m and 7.5 m. In the case when the rupture started in the Tokai/Tonankai segment (see

case 3-16 in **Table S4**, **Fig. S7**), the afterslip of the following Nankai asperity eroded part of the preceding Tokai/Tonankai asperity that had been healing, because the small L led to a weaker barrier effect (**Fig. S7a, b**). As a result, the stress remained higher at the afterslip front than in the surroundings (**Fig. S7c–f**), and in the next cycle the rupture started from the Tokai/Tonankai side.

On the other hand, when the rupture started in the Nankai segment (see case 3-13 in **Table S4**, **Fig. S8**), stress concentrations evolved equally in both the Tokai/Tonankai and Nankai asperities, and the rupture of the Nankai asperity came first by a very small amount of time (**Fig. S8a–d**). The large barrier effect of the belt-shaped area suppressed the afterslip erosion to the adjacent asperity (Tokai/Tonankai) in comparison to case 3-16 (**Fig. S8e, f**). After that, the rupture started from the lower end of the Tokai/Tonankai asperity adjacent to the belt (**Fig. S8g–j**). This reinforces the tendency of following event pairs to start with a Nankai event.

In cases 3-4 to 3-6 (**Table S4**; $L = 3.0$ m and belt width = 15 km), we found both patterns where the Tokai/Tonankai earthquake preceded the Nankai earthquake, and vice versa. The barrier effect of the belt-shaped area increased with L and the belt width. Because these cases used a slightly large L and a narrow belt, the barrier effect was moderate. Regardless of the polarity of the rupture sequence, preslip occurred first in the Tonankai asperity off Cape Shiono, and shear stress was concentrated around it (**Fig. S9b, f, B, F**). When the rupture cycle began in the Tonankai asperity, the preslip accelerated, nucleated, and resulted in a Tonankai earthquake (**Fig. S9e–h, E–H**). When the cycle began in the Nankai asperity, slip velocity (interplate coupling) needed to be high (low) at the eastern end of the Nankai asperity (compare **Fig. S9b** and **Fig. S9f**). As a result, slip accelerated at the eastern end of the Nankai asperity, leading to a Nankai earthquake (**Fig. S9d, D**). Since the barrier effect was moderate, it was moderately affected by the slip on the Tonankai side, and the slip distribution of the previous earthquake and the stress distribution after that were slightly different each time, and the stress state at the eastern end of the Nankai asperity changed. This difference in the generation pattern appears to be due to the slight difference in the stress state.

The historical evidence (**Fig. 1**) shows that Tokai/Tonankai earthquakes precede Nankai earthquakes, except perhaps in the 1498 Meio Nankai earthquake (doubtful) and the 1707 Hoei earthquake (when the two events were almost simultaneous); thus, we should probably set $L = 1.0$ m in the belt-shaped area. We cannot make this claim definitively, though, because the Tokai/Tonankai earthquake came first, even if $L = 7.5$ m was assigned to the belt, in cases when L was large in only the western part of the seismogenic zone (**Fig. S4e** and **Table S5** show information on

the ninth and tenth paired events). Consequently, to ensure that a Tokai/Tonankai earthquake precedes a Nankai earthquake with a time lag, it is necessary to assign large L to a belt-shaped area off Cape Shiono.

S2.3. Along-strike extent of rupture areas, the Showa Tonankai and Nankai earthquakes, and the Hyuganada earthquake

As for the target phenomenon 1a, especially in the Tokai/Tonankai segments, historical and observed evidence revealed that the eastern edges of the rupture of three most recent events (the 1707 Hoei, 1854 Ansei, and 1944 Showa events) were bound at Cape Omaezaki (1707), Suruga Bay (1854), and Lake Hamana (1944), respectively (Matsu'ura 2012; Earthquake Research Committee 2013) (**Fig. 2**). The variety of eastern extent of rupture area could not be modeled with the spatial distribution of L just shown in **Fig. S4e**, nor by assigning a single large L value in the Tokai district, expecting it to act as a barrier (Hirose and Maeda 2013). Thus, we assigned two different large L values to the Tokai district (**Fig. S4f**, regions including points 1 and 2). The resulting time series in the regions of points 1–5 (**Fig. S10**) showed that recurrence intervals of earthquakes at point 3 were about 90, 100, and 130 years. At point 2, the peak of slip velocity was reduced in one of three earthquakes, and the peak of slip velocity was much lower at point 1 than at points 2 or 3. Although this parameter tuning was partly insufficient because interplate coupling rate at point 1 was inconsistent with observations (Nishimura et al. 2018), it suggests that target phenomena 1a and the specifics of the historic Showa earthquakes (target phenomenon 1e) was almost reproduced by applying the spatial distribution of L as shown in **Fig. S4f**.

The 1946 Showa Nankai earthquake started off Cape Shiono, and large slips occurred beneath the Shikoku coast (Baba and Cummins 2005) (**Fig. 2a**). We adopted a heterogeneous distribution of L (**Fig. S4g**) because a uniform L did not reproduce the large slips beneath coastal Shikoku and in consideration of the Hyuganada earthquake. This change enabled us to generally reproduce the extent of coseismic slip of the Showa Nankai earthquake (target phenomenon 1e), although this parameter tuning was still insufficient. Furthermore, mega-earthquakes that ruptured the shallower (point 5) and deeper (point 4) zones simultaneously were also simulated at a rate of once in 300 years (**Fig. S10**), slightly more frequent than the 400–600 years of target phenomenon 1d.

When we assigned a large σ^{eff} value (60 MPa) to the asperity area in the northern Hyuganada and tuned L so that the nucleation size approached the asperity size (50 km \times 50 km) (point 6 in **Fig. 4** and **Table 2**), $M_w \sim 7.5$ events were simulated at somewhat longer recurrence intervals (up to 292 years).

S2.4. Parameter tuning to reproduce the slip-deficit rate distribution

Here we explain the reproduction of slip-deficit rates, target phenomenon 3 (Nishimura et al. 2018). There are several local slip-deficit rate maxima along the Nankai Trough and regions of low slip-deficit rate off the Shima Peninsula, Cape Shiono, Cape Muroto (Tosabae seamount), and Cape Ashizuri. We found that the fit to the observed low-rate region beneath Tosabae qualitatively improved (**Fig. S11**) when we assigned there a large L (and small σ^{eff}) shown in **Fig. S4i, k** rather than those in **Fig. S4h, j**.

We applied the same change to the area off the Shima Peninsula. As a result, occurrence intervals of great earthquakes decreased from 90–130 years to 60–105 years. These occurrence intervals are not consistent with the historical record (**Fig. 1**); therefore, we increased $|a - b|$ in the seismogenic zone, testing both $a - b = -0.0025$ and -0.003 . We adopted the latter value, which produced occurrence intervals of 90–190 years.

S2.5. Summary of parameter tuning

Though parameter tuning by trial and error, we were able to find heterogeneous spatial distributions of L and σ^{eff} (**Fig. 4e, f**) that made it possible to reproduce observations to some extent. However, during this procedure the frictional parameter a was held constant, and b was changed at the depth of 30 km by a simple step function. Note that laboratory experiments have shown that both a and b depend on slip velocity, temperature (depth), and σ^{eff} (e.g., Blanpied et al. 1998; Sawai et al. 2016). Therefore, a more realistic model should incorporate not only spatial heterogeneity of L and σ^{eff} but also spatial heterogeneity of a and b and the temporal variation of parameters. In addition, parameters need to be better constrained by monitoring data for the state of the interplate boundary obtained with high-resolution instruments.

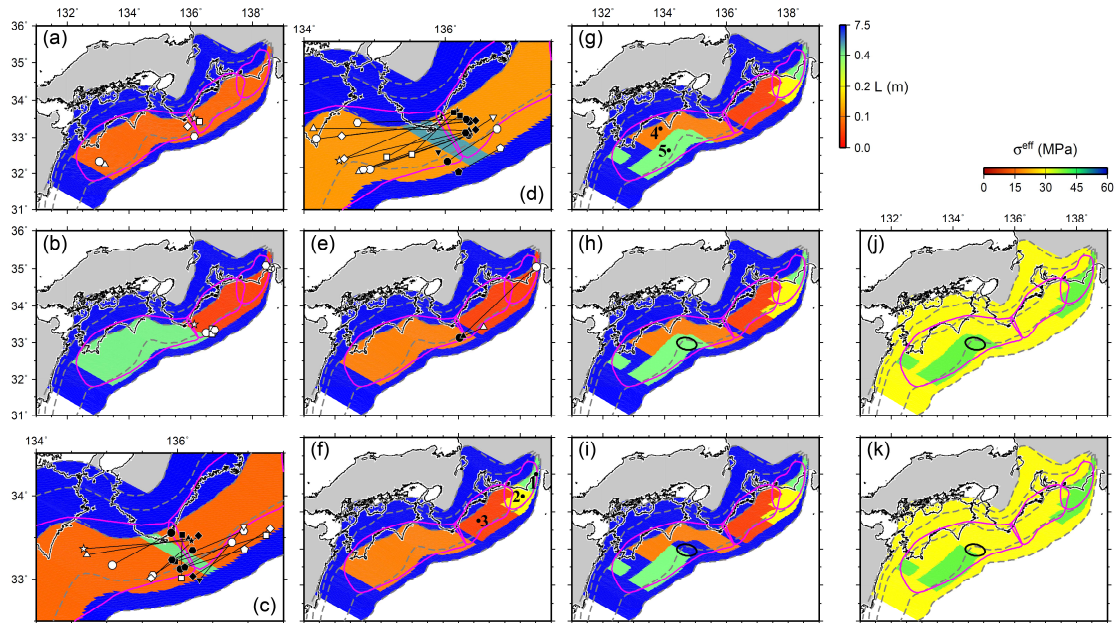


Fig. S4 Examples of characteristic displacement L and effective normal stress σ^{eff} . Symbols indicate the starting points of earthquakes. Open and solid symbols connected by a line in (c–e) indicate preceding and following events, respectively. Parameter distributions of L are based on (a) case 1-3 in Table S2, (b) case 2-5 in Table S3, (c) case 3-7 in Table S4, (d) case 3-15 in Table S4, and (e) case 4-1 in Table S5 for reproducing the time lag between Tokai/Tonankai and Nankai earthquakes. (f) An example of a spatial distribution of L used to try to reproduce rupture variations in the Tokai area. (g) An example of a spatial distribution of L used to try to reproduce rupture variations in the Nankai area. (h–k) Examples of spatial distributions of L and σ^{eff} used to try to reproduce low slip-deficit rates at the Tosabae seamount (black ellipse) (see Fig. S11). See Figure 2 for other symbols.

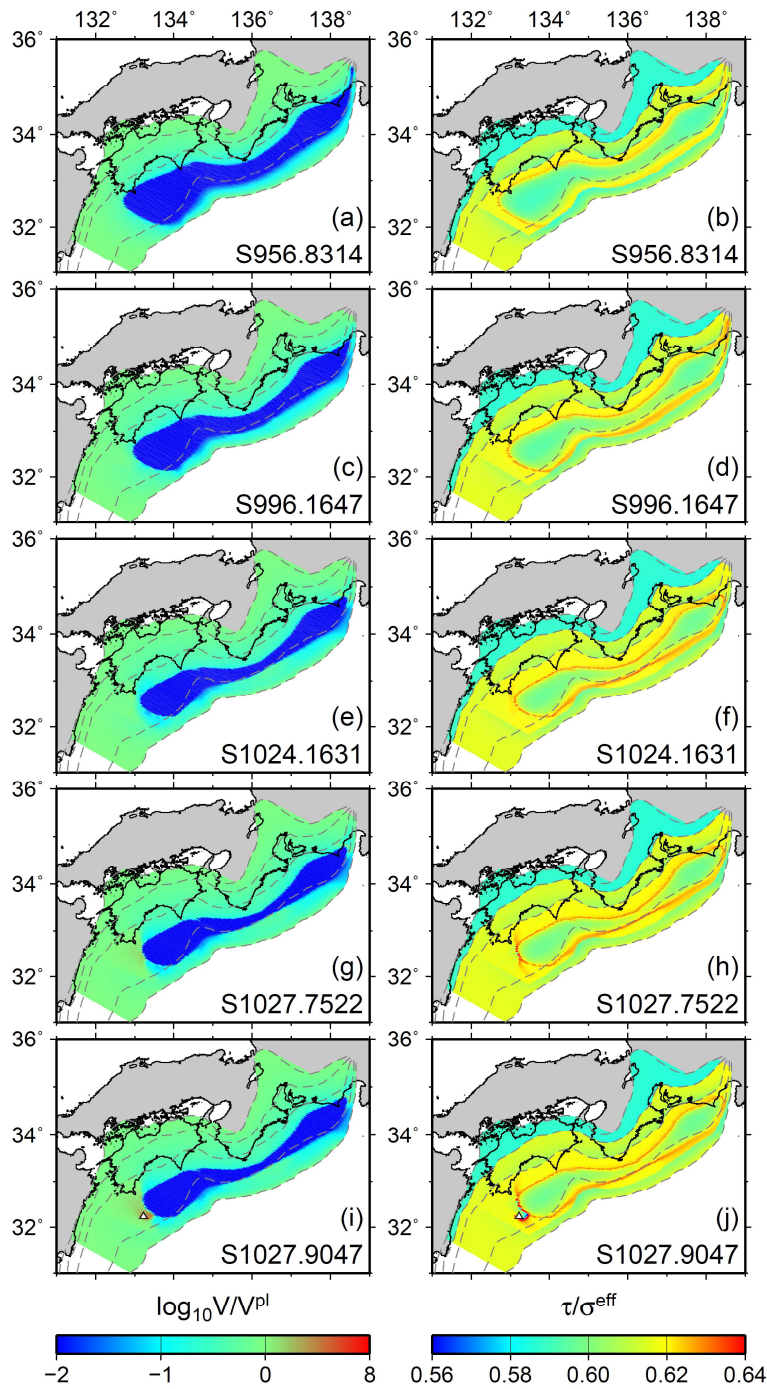


Fig. S5 Snapshots of (left) slip velocity and (right) shear stress on the plate interface for case 1-2 in Table S2. Slip velocity and shear stress are normalized by plate convergence rates and normal stress, respectively. (a, b) ~ 70 years before, (c, d) ~ 30 years before, (e, f) ~ 4 years before, (g, h) Immediately before, and (i, j) at the start of an earthquake with the starting point off Cape Ashizuri (epicenter shown by triangle). Other symbols are as shown in Figure 2.

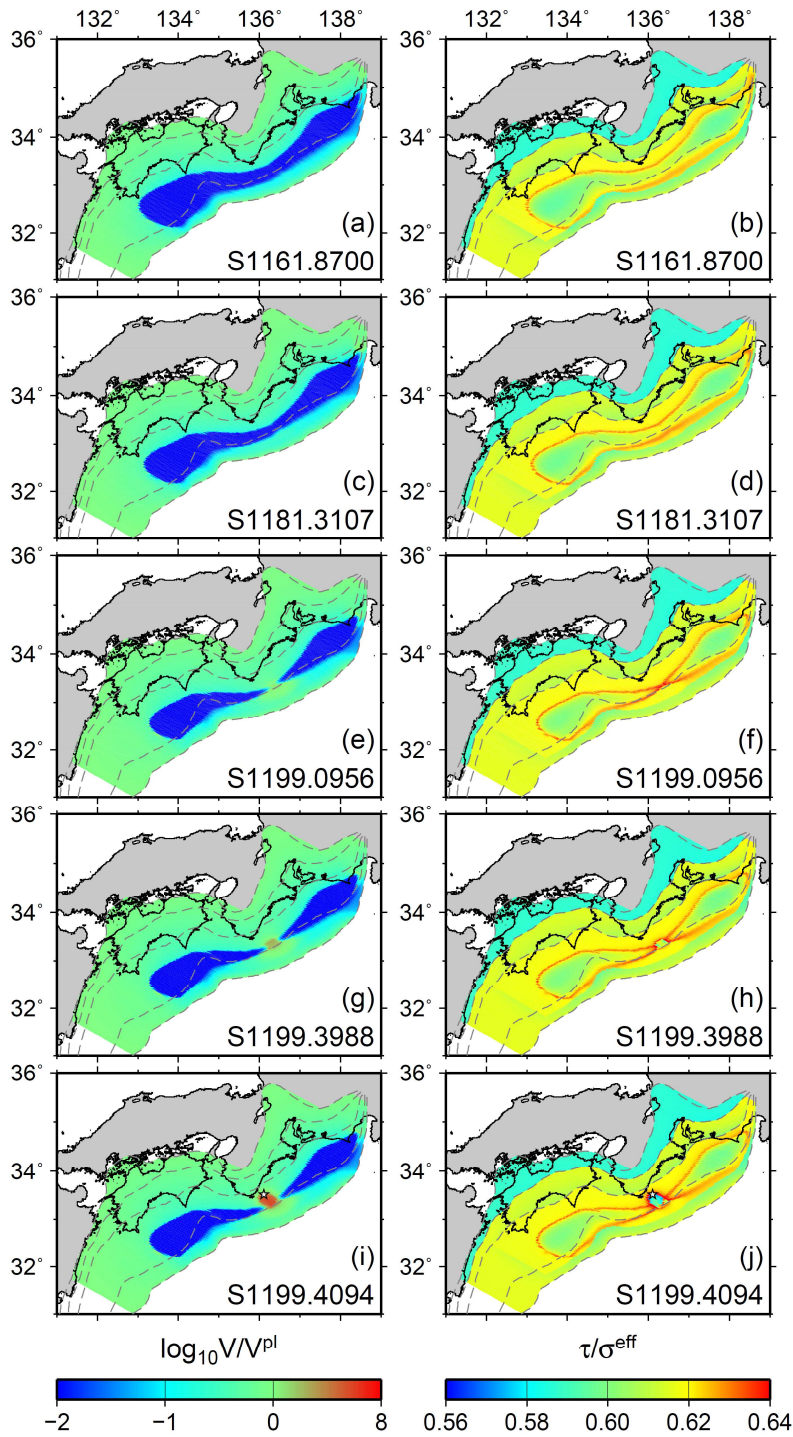


Fig. S6 Snapshots of (left) slip velocity and (right) shear stress on the plate interface for case 1-3 in Table S2. Slip velocity and shear stress are normalized by plate convergence rates and normal stress, respectively. (a, b) ~40 years before, (c, d) ~20 years before, (e, f) shortly before, (g, h) Immediately before, and (i, j) at the start of an earthquake with the starting point off Cape Shiono (epicenter shown by star).

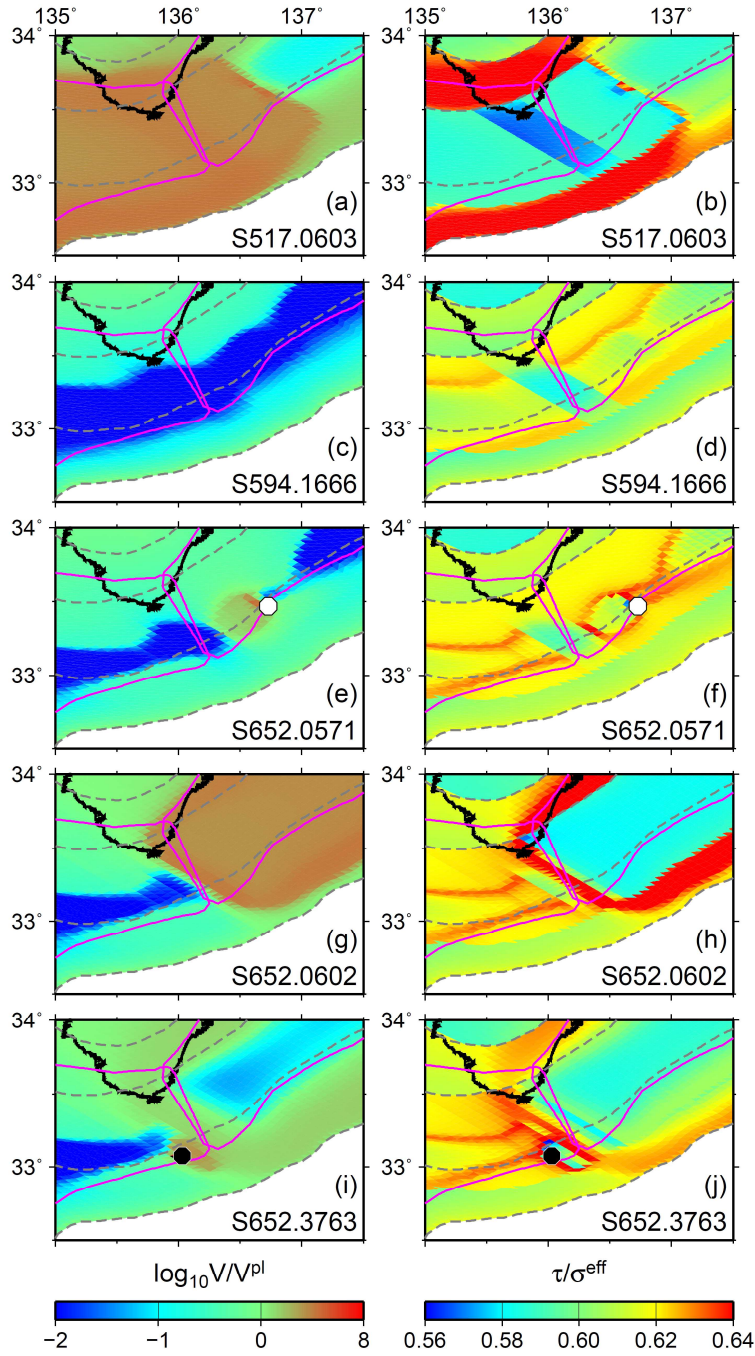


Fig. S7 Snapshots of (left) slip velocity and (right) shear stress on the plate interface for case 3-16 in Table S4. Slip velocity and shear stress are normalized by plate convergence rates and normal stress, respectively. (a, b) Immediately after the ninth Nankai earthquake. (c, d) Between the ninth and tenth earthquakes. (e, f) At the start of the tenth Tonankai earthquake; the open octagon is its epicenter. (g, h) Immediately after the tenth Tonankai earthquake. (i, j) At the start of the tenth Nankai earthquake; the solid octagon is its epicenter.

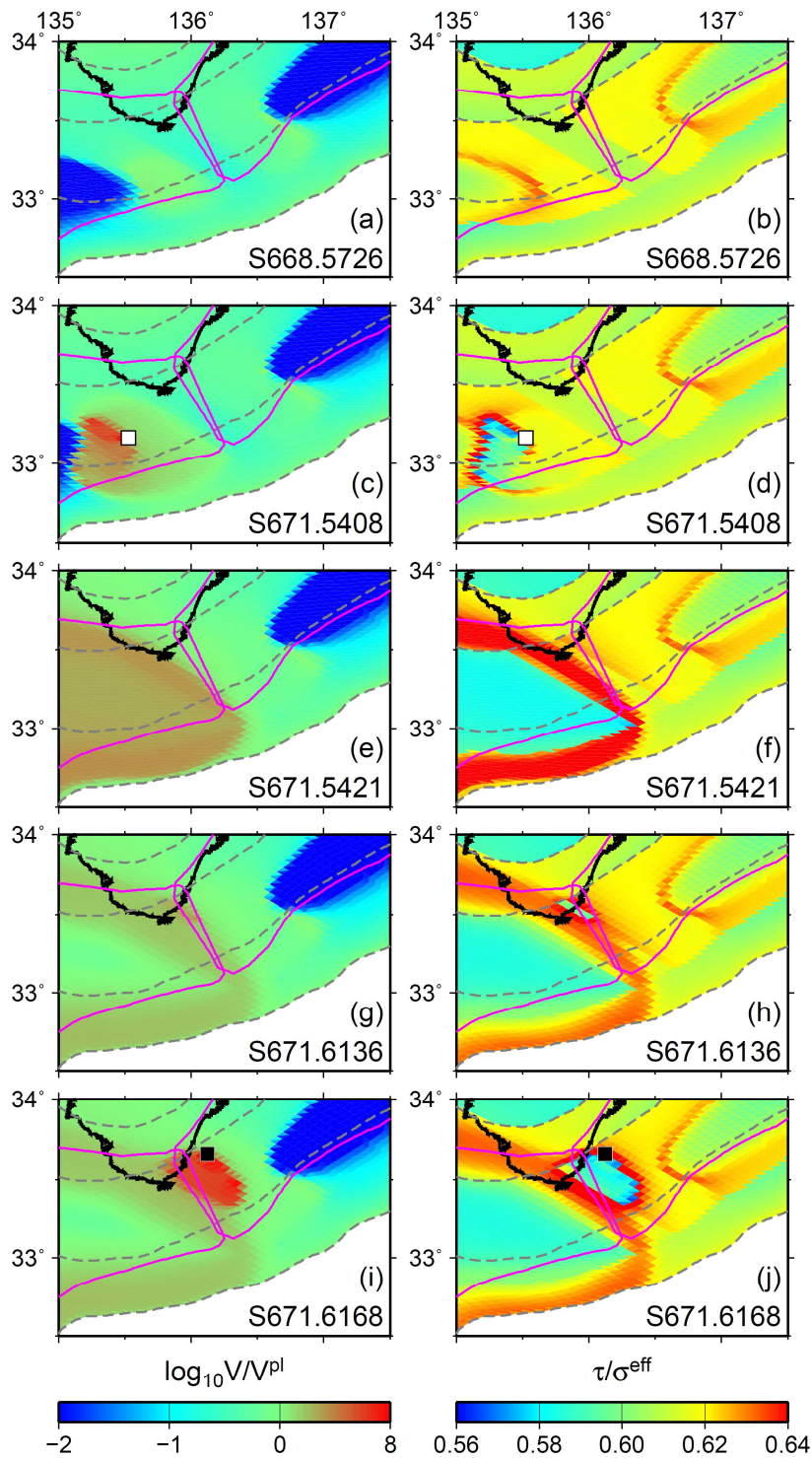


Fig. S8 Snapshots of (left) slip velocity and (right) shear stress on the plate interface for case 3-13 in Table S4. (a, b) Between the ninth and tenth earthquakes. (c, d) At the start of the tenth Nankai earthquake; the open square is its epicenter. (e, f) Immediately after the tenth Nankai earthquake. (g, h) Between the tenth Nankai and Tonankai earthquakes. (i, j) At the start of the tenth Tonankai earthquake; the solid square is its epicenter.

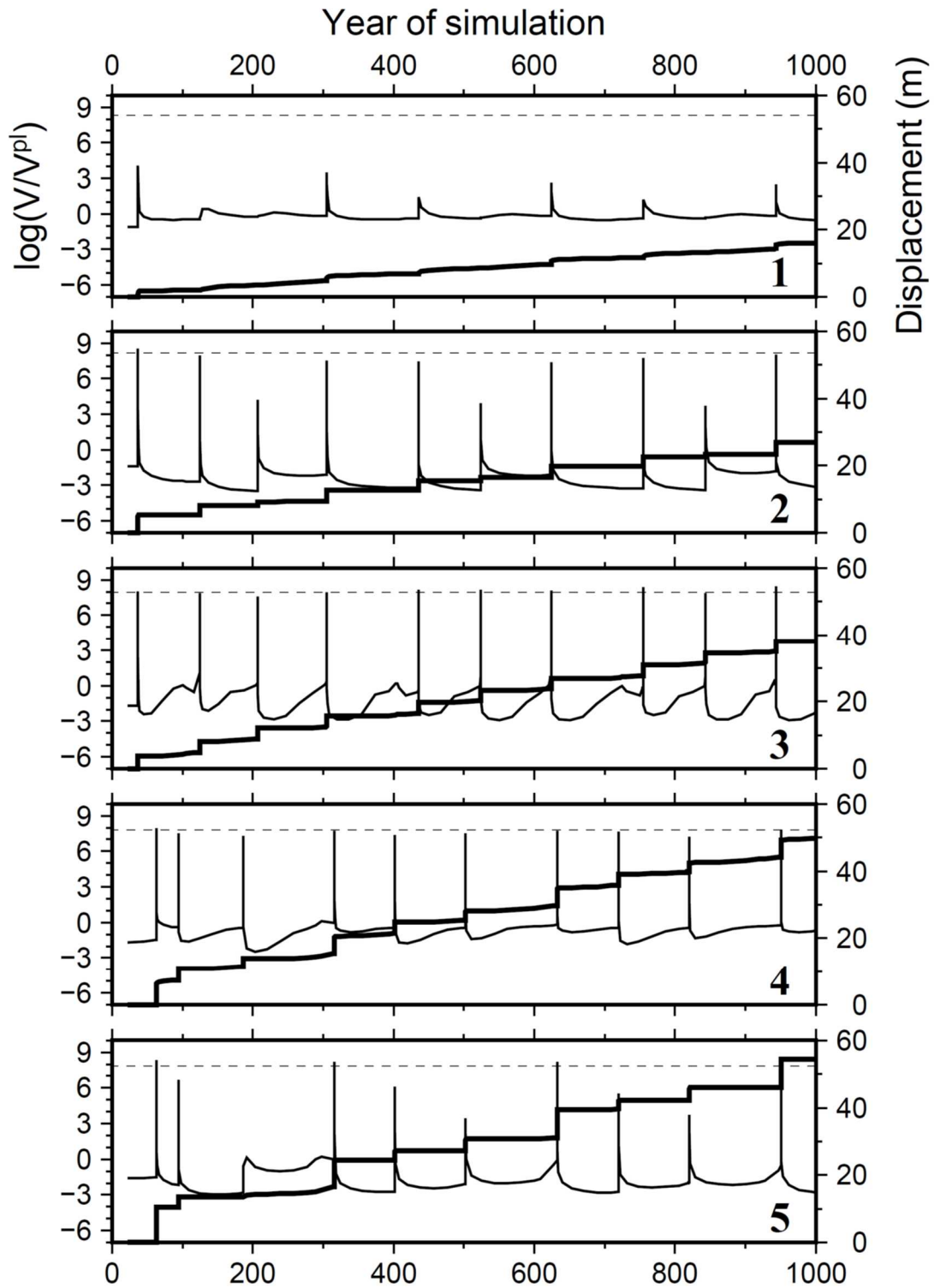


Fig. S10 Time evolution of slip velocity normalized by the plate convergence rate (thin line) and cumulative slip displacement (thick line) at locations marked by points 1–5 in Figure S4. The dashed line in each panel corresponds to a slip velocity of 0.1 m/s, the threshold for earthquakes.

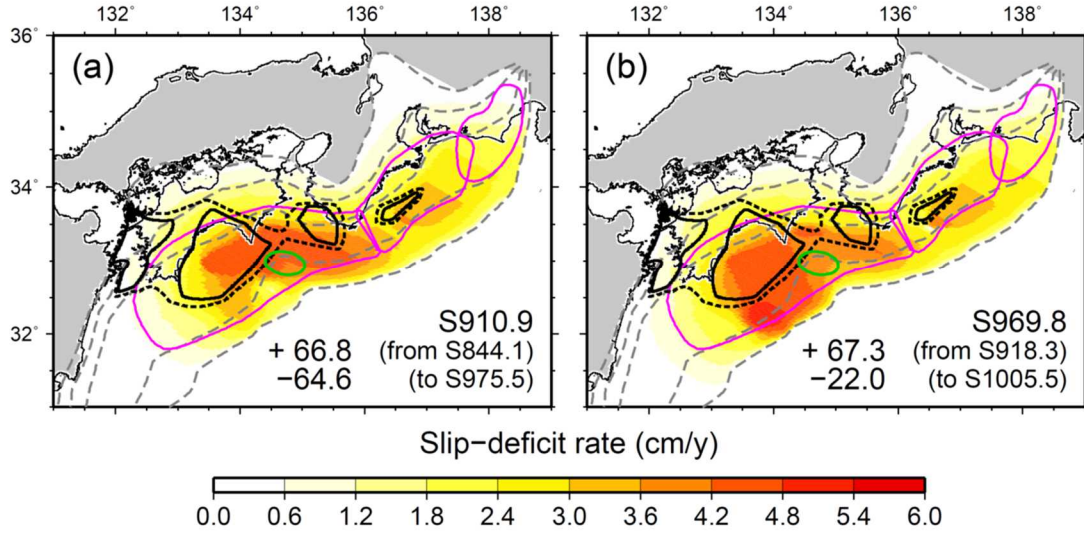


Fig. S11. Spatial distribution of the slip-deficit rate on the plate interface at ~ 70 years after a Nankai earthquake with the parameter distributions in (a) Figure S4h, j and (b) Figure S4i, k. The solid and broken black lines are the 3.0 and 2.4 cm/y contours of slip-deficit rate (standard error < 2.0 cm/y), respectively (Nishimura et al. 2018). Numbers at lower right indicate the elapsed time from the start of the simulation, the elapsed time from a previous earthquake, and leading time to the next earthquake, respectively. Green ellipse indicates the Tosabae seamount (Kodaira et al. 2000).

Table S1 The range of parameters at points 1–12 in Figure 4e, f tested in our best simulation. See Table 2 for its preferred values.

Point (Fig. 4e, f)	L (m)	σ^{eff} (MPa)	h^* (km)	a	b	$a - b$
1	0.05–0.60	30–40	25–150	0.005	0.007–0.008	-0.002 to -0.003
2	0.05–0.50	30–40	25–71	0.005	0.007–0.008	-0.002 to -0.003
3	0.05–0.50	30–41	24–60	0.005	0.007–0.008	-0.002 to -0.003
4	0.05–0.18	30–42	25–60	0.005	0.007–0.008	-0.002 to -0.003
5	0.05–0.80	30–43	25–200	0.005	0.007–0.008	-0.002 to -0.003
6	0.05–0.25	30–80	25–60	0.005	0.007–0.008	-0.002 to -0.003
7	7.5	30	2500–3750	0.005	0.007–0.008	-0.002 to -0.003
8	0.0033–7.5	1.5–30	22–3750	0.005	0.007–0.008	-0.002 to -0.003
9	0.0090–7.5	4–30	23–3750	0.005	0.007–0.008	-0.002 to -0.003
10	0.0310–7.5	10–30	31–3750	0.005	0.007–0.008	-0.002 to -0.003
11	0.0100–7.5	3–30	25–3750	0.005	0.007–0.008	-0.002 to -0.003
12	7.5	30	–	0.005	0.002–0.003	0.002–0.003

Table S2 Parameters applied in this study with $a = 0.005$, $b = 0.007$, and $\sigma^{\text{eff}} = 30$ MPa in the seismogenic zone, corresponding to Figure S4a. M_w is the magnitude of the tenth earthquake in the simulation, and T_r is the recurrence interval between the ninth and tenth earthquakes.

Case	L (m)	h^* (km)	M_w	T_r (years)	Starting point	Symbol (Fig. S4a)
1-1	0.05	25.0	8.5	91	Off Cape Ashizuri	circle
1-2	0.06	30.0	8.5	117	Off Cape Ashizuri	triangle
1-3	0.08	40.0	8.6	136	Off Cape Shiono	star
1-4	0.10	50.0	8.6	145	Off Cape Shiono	square
1-5	0.12	60.0	8.6	153	Off Cape Shiono	hexagon
1-6	0.14	70.0	8.6	159	Off Cape Shiono	diamond

Table S3 Parameters applied in this study corresponding to Figure S4b. M_w is the magnitude range of the tenth and eleventh earthquakes, T_r is the range in recurrence interval from the ninth to the tenth and from the tenth to the eleventh earthquakes, and ΔT is the time lag between Tokai/Tonankai and Nankai earthquakes.

Case	L (m)		h^* (km)		M_w	T_r (years)	ΔT^\dagger (days)	Starting point	Symbol (Fig. S4b)
	Nankai	Tokai/Tonankai	Nankai	Tokai/Tonankai					
2-1	0.10	0.05	50.0	25.0	8.4–8.5	90–137	0	Eastern end/off Cape Shiono	circle
2-2	0.20	0.05	100.0	25.0	8.4–8.5	92–129	0	Eastern end/off Cape Shiono	triangle
2-3	0.40	0.05	200.0	25.0	8.1–8.7	86–98	0	Eastern end/off Cape Shiono	star
2-4	0.60	0.05	300.0	25.0	8.0–8.1	70–95	–	Off Cape Shiono	square
2-5	0.80	0.05	400.0	25.0	8.1	94–109	–	Eastern end/off Cape Shiono	hexagon

†: No Nankai earthquake appeared at $L \geq 0.6$ m in the Nankai segment.

Table S4 Parameters applied in this study corresponding to Figure S4c, d. ΔT is the time lag between the tenth Tokai/Tonankai and Nankai earthquakes; a range for ΔT means that the time lag between the eleventh Tokai/Tonankai and Nankai earthquakes is included.

Case	Width [†] (km)	L^{\dagger} (m)	$L^{\dagger\dagger}$ (m)	ΔT (days)	Order of rupture	Symbol (Fig. S4c, d)‡
3-1	15	7.5	0.08	0.7	Nankai → Tokai/Tonankai	circle
3-2	15	7.5	0.10	0.5	Nankai → Tokai/Tonankai	triangle
3-3	15	7.5	0.12	0.5	Nankai → Tokai/Tonankai	star
3-4	15	3.0	0.08	0.7–15	Nankai ↔ Tokai/Tonankai	square
3-5	15	3.0	0.10	0.4–9	Nankai ↔ Tokai/Tonankai	hexagon
3-6	15	3.0	0.12	0.2–7	Nankai ↔ Tokai/Tonankai	diamond
3-7	15	1.0	0.08	3	Nankai ← Tokai/Tonankai	octagon
3-8	15	1.0	0.10	1.5	Nankai ← Tokai/Tonankai	pentagon
3-9	15	1.0	0.12	0.7	Nankai ← Tokai/Tonankai	inverse triangle
3-10	25	7.5	0.08	15–18	Nankai → Tokai/Tonankai	circle
3-11	25	7.5	0.10	15–18	Nankai → Tokai/Tonankai	triangle
3-12	25	7.5	0.12	15	Nankai → Tokai/Tonankai	star
3-13	25	3.0	0.08	11–29	Nankai → Tokai/Tonankai	square
3-14	25	3.0	0.10	7–18	Nankai → Tokai/Tonankai	hexagon
3-15	25	3.0	0.12	7–15	Nankai → Tokai/Tonankai	diamond
3-16	25	1.0	0.08	117	Nankai ← Tokai/Tonankai	octagon
3-17	25	1.0	0.10	80	Nankai ← Tokai/Tonankai	pentagon
3-18	25	1.0	0.12	73	Nankai ← Tokai/Tonankai	inverse triangle

†: Value set at the border between the Tokai/Tonankai and Nankai segments.

††: Value set in the seismogenic zone.

‡: Cases 3-1 to 3-9 are in Figure S4c and cases 3-10 to 3-18 are in Figure S4d.

Table S5 Parameters applied in this study corresponding to Figure S4e. ΔT is the range in time lag of the ninth and tenth pairs of Tokai/Tonankai and Nankai earthquakes.

Case	Width [†] (km)	L^{\dagger} (m)	$L^{\dagger\dagger}$ (m)		ΔT (days)	Order of rupture
			Nankai	Tonankai		
4-1	15	7.5	0.1	0.05	15–29	Nankai ← Tokai/Tonankai

†: Value set at the border between the Tokai/Tonankai and Nankai segments.

††: Value set in the seismogenic zone.